Colloids and Surfaces B: Biointerfaces 161 (2018) 339–346

Contents lists available at ScienceDirect

Colloids and Surfaces B: Biointerfaces

journal homepage: www.elsevier.com/locate/colsurfb

Protocols

Improving sensitivity of magnetic resonance imaging by using a dual-targeted magnetic iron oxide nanoprobe

Ling Chen[a], Jun Xie[a,b], Haoan Wu[a], Fengchao Zang[c], Ming Ma[a], Zichun Hua[d,**], Ning Gu[a,*], Yu Zhang[a,*]

[a] State Key Laboratory of Bioelectronics, Jiangsu Key Laboratory for Biomaterials and Devices, School of Biological Science and Medical Engineering & Collaborative Innovation Center of Suzhou Nano Science and Technology, Southeast University, Nanjing 210096, PR China
[b] School of Life Science, Jiangsu Normal University, Xuzhou 221116, PR China
[c] Jiangsu Key Laboratory of Molecular and Functional Imaging, Medical School, Southeast University, Nanjing 210096, PR China
[d] State Key Laboratory of Pharmaceutical Biotechnology, School of Life Sciences, Nanjing University, Nanjing 210023, PR China

ARTICLE INFO

Article history:
Received 17 July 2017
Received in revised form 19 October 2017
Accepted 21 October 2017
Available online 24 October 2017

Keywords:
Fe_3O_4 magnetic nanoparticles
Bispecific nanoprobe
Magnetic resonance molecular imaging
Sensitivity

ABSTRACT

Developing an ultrasensitive and high-efficient molecular imaging probe for detection of malignant tumors is extremely needed in clinical and remains a big challenge. Here, we report a novel bispecific nanoprobe for dual-targeted T2-weighed magnetic resonance imaging (MRI) of COLO-205 colorectal cancer in vivo. First, the magnetic iron oxide nanoparticles (Fe_3O_4@OA) were synthesized by a thermal decomposition method. Then, PEGylation of the hydrophobic Fe_3O_4@OA was implemented by amphiphilic DSPE-PEG2000-COOH, producing water-soluble nanoparticles (Fe_3O_4@PEG). Lastly, arginine-glycine-asparticacid-tumornecrosis factor-related apoptosis-inducing ligand (RGD-TRAIL), a bispecific fusion protein, was conjugated with the nanoparticle to construct molecularly multi-targeted nanoprobe, which was defined as Fe_3O_4@RGD-TRAIL. This Fe_3O_4@RGD-TRAIL was proven to exhibit extremely high relaxation property ($r_2 = 534\,mM^{-1}s^{-1}$) and saturation magnetization value ($M_s = 92$ emu/g Fe). In vitro studies showed its dual-targeting combination capacity, favorable biocompatibility and strong ability to resist against the non-specific phagocytosis. Owing to these excellent advantages, high sensitive and efficient imaging of tumor was achieved in vivo. Therefore, this RGD-TRAIL conjugated nanoprobe could be developed as a multi-targeted contrast enhancement agent for magnetic resonance molecular imaging in detection of cancer.

1. Introduction

Over the past decade, nanomedicine has emerged and been a new interdisciplinary field [1] that applied to medical diagnosis and treatment. Among a variety of nanomaterials, magnetic iron oxide nanoparticles as MRI contrast agents have been approved by FDA for use in clinical for years [2,3]. Subsequently, magnetic nanoparticles have received tremendous attention in various research areas among which MRI for cancer detection is one of the most important applications. Initially, iron oxide nanoparticles were designed to passively target the tumors via enhanced permeability and retention (EPR) effect [4–7]. With the development of molecular imaging, various ligands have been modified onto the surface of the iron oxide nanoparticles to specifically target the tumors with upregulated specific receptors (include EGFR, HER2, folate receptor, $\alpha_v\beta_3$ integrin) which are rarely expressed by healthy tissues [8–11]. To further increase the detecting sensibility and efficiency, bispecific nanoparticles have also been developed for tumor imaging [12].

As to be an ideal T2-weighted MR contrast agent for effective in vivo application, the magnetic iron oxide nanoparticles should be exploited with high performance, including superior magnetism, favorable biocompatibility and stability, and long blood circulation time. A thermal decomposition method for synthesis of iron oxide nanoparticles offers great advantages over aqueous precipitation method, involving higher crystallinity, monodispersity, favorable morphology and controlled size [13–16]. Nevertheless, the products of thermal decomposition method are hydrophobic, further surface modification is needed to enable the nanoparticles become water-soluble and prevent aggregation. PEGylation is known as a common method for evading phagocytosis by the reticuloendothe-

* Corresponding authors.
** Corresponding author.
E-mail addresses: huazc@nju.edu.cn (Z. Hua), guning@seu.edu.cn (N. Gu), zhangyu@seu.edu.cn (Y. Zhang).

https://doi.org/10.1016/j.colsurfb.2017.10.059
0927-7765/

lial system (RES). Phospholipid-polyethylene glycol (DSPE-PEG) approved by FDA is one of the most biocompatible coating materials. After encapsulating the nanoparticles, the outer PEG chain allows the nanoparticles to be dispersed stably in water solution and have a relatively long blood circulation time [17]. Further more, specific ligands could be covalently bonded onto the nanoparticles through the functional group of DSPE-PEG.

Although extensive studies proved the effectiveness of passive targeting via EPR effect both in tumor imaging and therapy [18–20], the tumor microenvironment especially tumor vasculature is highly heterogeneous and continuously evolving [21], resulting in heterogeneous extravasation and delivery of nanomaterials. One possible way to reduce the influence produced by heterogeneity of tumor microenvironment, improve targeting efficiency and achieve more sensitive diagnosis is to simultaneously target multiple tumor-associated receptors [12]. Using a bispecific ligand instead of two independent ligands for nanoparticle decoration not only simplifies the conjugation process but also avoids the difference of targeting combination induced by different properties of two ligands. Thus, the selection of an appropriate ligand is a key event to realize sensitive detection of cancer disease, and more over to evaluate the therapeutic efficacy aiming at the corresponding receptor. Herein, Arginine-glycine-aspartic acid-tumor necrosis factor-related apoptosis-inducing ligand (RGD-TRAIL) is considered to be a promising ligand for magnetic resonance molecular imaging. RGD-TRAIL is a bispecific fusion protein which can simultaneously target to intergrin overexpressed on tumor neovascular endothelium and several tumor cells via RGD fragment and death receptors (DR4/TRAIL-R1, DR5/TRAIL-R2) expressed by various tumor cells via TRAIL, inducing cell death [22]. Therefore, RGD-TRAIL conjugated nanoparticles can be not only applied for tumor diagnosis, but also for guidance of the treatment by targeted imaging of neovascularization and death receptors.

In this study, we developed a bispecific PEGylated iron oxide nanoprobe with high performance. It was synthesized by thermal decomposition method and encapsulated with DSPE-PEG-COOH. The surface of the nanoparticle was further decorated with a dual-targeting ligand called RGD-TRAIL to form a molecular nanoprobe for targeting and magnetic resonance imaging of COLO-205 colorectal cancer. Our work demonstrated that this T2-weighed nanoprobe possessed excellent magnetism, high relaxivity, remarkable biocompatibility and outstanding sensitivity and precision for tumor MRI imaging.

2. Materials and method

2.1. Materials

$Fe(acac)_3$, oleic acid (OA) and oleylamine (OAm) were bought from Aladdin (China). Benzyl ether was obtained from Alfa aesar (USA). DSPE-PEG2000-COOH was bought from A.V.T. Pharmaceutical L.T.D. (China). EDC·HCL and MES was purchased from Sigma-Aldrich. NHS was procured from damas-beta (China). RGD-TRAIL protein, molecular weight of ≈21 000 Da, was provided by Nanjing University State Key Laboratory for Medical Biotechnology [22]. DMEM-1640, fetal bovine serum (FBS) and trypsin-EDTA were purchased from commercial sources. COLO-205 cells, HUVECs and RAW264.7 macrophages were obtained from the Type Culture Collection of the Chinese Academy of Sciences (China).

2.1.1. Synthesis of Fe_3O_4@OA

The oleic acid (OA) coated iron oxide nanoparticles (Fe_3O_4@OA) were synthesized by a thermal decomposition method [13]. In detail, 2 mmol $Fe(acac)_3$ was placed in a 100 ml three-neck flask with 20 ml benzyl ether, 7.5 mmol OA and 4.5 mmol OAm were added and the mixture was stirred by a flow of N_2. The reactants were heated from room temperature to 220 °C in 1 h and kept at 220 °C for 1 h, then heated to 290 °C and maintained for 30 min. Lastly, the product was precipitated on the magnet and washed 3 times using ethanol, and was then dispersed in 10 ml chloroform.

2.1.2. Synthesis of Fe_3O_4@PEG and Fe_3O_4@RGD-TRAIL

Fe_3O_4@PEG was synthesized according to a previous report with modification [23]. 40 mg DSPE-PEG2000-COOH powder was added to a 25 ml round-bottom flask and dissolved in 3 ml chloroform, 10 mg (Fe content) Fe_3O_4@OA was then mixed and 7 ml deionized water was added together. The mixture was rotarily evaporated at 70 °C until the chloroform was completely vaporized. The monodispersed water soluble iron oxide nanoprobes (Fe_3O_4@PEG) were obtained.

In the fabrication of Fe_3O_4@RGD-TRAIL, RGD-TRAIL protein molecules were chemically conjugated onto Fe_3O_4@PEG. Firstly, 10 mg Fe_3O_4@PEG were suspended in MES buffer (0.02 M, pH = 5.4) using an ultrafiltration centrifuge tube (100 kDa MWCO, 4500 rpm, 5 min). Carboxyl groups on the surface of Fe_3O_4@PEG were then activated by EDC (27 mg) and NHS (24 mg) in 20 ml MES buffer. The reactants were then stirred for 25 min at room temperature. The reaction mixture was ultrafiltered with deionized water for 3 times and then dispersed in borate buffer (0.02 M, pH = 8.0) with certain RGD-TRAIL protein molecules, and stirred continuously at room temperature for 4 h. Free RGD-TRAIL was removed by ultrafiltration with deionzed water, and measured by BCA kit. The product was lastly filtered using a 220 nm filtering membrane and stored in 4 °C.

2.1.3. Synthesis of Fe_3O_4@DMSA

DMSA molecules were modified onto hydrophobic Fe_3O_4@OA through ligand exchange, making Fe_3O_4@DMSA water soluble [24]. In detail, 15 mg (Fe content) Fe_3O_4@OA was dispersed in 15 ml hexane and mixed with 50 mg DMSA dissolving in 40 ml acetone. The mixture was added into a 100 ml three-neck flask and 300 μl triethylamine was then added. After 4 h fast stirring at 55 °C, the product was washed 3 times with ethanol on the magnet and dispersed in 10 ml deionized water. After purified by dialysis for 3 days, the Fe_3O_4@DMSA was obtained and stored in 4 °C.

2.2. Characterization of Fe_3O_4@PEG and Fe_3O_4@RGD-TRAIL

The morphology of Fe_3O_4@OA, Fe_3O_4@PEG and Fe_3O_4@RGD-TRAIL was examined using TEM (Tokyo JEOL, Japan). The hydrodynamic size distribution was measured with a particle size analyzer (Malvern ZS90, UK). The magnetism was observed by a vibrating sample magnetometer (VSM, Lakeshore 7407, USA). The iron concentration of the iron oxide nanoparticles was measured by the 1, 10-phenanthroline spectrophotometric method on a UV–vis spectrophotometer (UV-3600, Shimadzu, Japan) [24,25]. The RGD-TRAIL protein content coupling on the nanoparticle was evaluated by BCA kit using a microplate reader (BioTek ELx808, USA). The T2-weighted MR imaging and relaxation property of Fe_3O_4@PEG and Fe_3O_4@RGD-TRAIL were carried out on a clinical 1.5 T MR scanner (Avanto, Siemens, Germany).

2.3. Cellular experiments

COLO-205 cells and HUVECs were cultured in RPMI-1640 medium supplemented with 10% FBS and 1% penicillin/streptomycin. RAW264.7 macrophages were maintained in DMEM medium supplemented with 10% FBS and 1% penicillin/streptomycin. All cells were cultured in humidified incubators maintained at 37 °C with 5% CO_2.

To investigate the targeted delivery of Fe_3O_4@RGD-TRAIL, cellular targeting experiments were performed with COLO-205 cells expressing DR4/DR5 and $\alpha_v\beta_3$-positive HUVECs. Proper concentration of COLO-205 cells were immobilized onto a slide using a cell smear centrifuge, and fixed with 4% paraformaldehyde, and then PBS, Fe_3O_4@PEG and Fe_3O_4@RGD-TRAIL were dropped to the cells respectively. After 6 h incubation at 37 °C, the cells were washed 3 times with PBS. Prussian blue staining was used to determine the presence of iron on the cytomembrane followed by counter staining with nuclear fast red. Similarly, HUVECs were cultured in a 6-well plate with 2×10^5 cells per well, incubated with PBS, Fe_3O_4@PEG and Fe_3O_4@RGD-TRAIL at the concentration of 100 μg Fe/ml for 12 h. The treatment was the same as above.

To evaluate the cytotoxicity of Fe_3O_4@PEG and Fe_3O_4@RGD-TRAIL, CCK8 assay was carried out in different cell line (COLO-205 and HUVEC). The cells were seeded onto 96-well plates with 1×10^4 cells per well and grown overnight, and subsequently incubated with the probes at a series of concentrations (0–60 μg Fe per ml) for 24 h. The relative viabilities of these cells versus untreated cells were determined by the CCK8 assay.

Raw264.7 macrophages were used to detect the anti-phagocytosis of the probes. Comparatively, the macrophages were treated with Fe_3O_4@PEG, Fe_3O_4@RGD-TRAIL and Fe3O4@DMSA at different concentrations of 50 and 100 μg Fe per ml for 4 h. Nuclear fast red and Prussian blue double staining were followed to display the cellular uptake of these probes.

2.4. Animal protocol

BALB/c nude mice (4–6 weeks of age, 18–20 g in weight) were purchased from the Model Animal Research Center of Southeast University. All animal procedures were performed in compliance with the animal experimentation guidelines of the Animal Research Ethics Board of Southeast University. To establish the experimental model of colon tumor, COLO-205 cells ($\sim 5 \times 10^6$ cells in 200 μl PBS) were subcutaneously injected into the right flanks of the nude mice. Ten days after injection, the mice were used for MR diagnostics when the tumor grew to probably 50 mm^3.

2.5. In vivo MRI experiments

A 7.0 T micro-MRI (PharmaScan, Brukers, Germany) was applied for in vivo MR imaging using a 38 mm circular coil and a mouse cradle. Before imaging, Mice were initially anesthetized with isoflurane. MR imaging was taken prior to tail vein injection and post injection of Fe_3O_4@PEG and Fe_3O_4@RGD-TRAIL (17.5 mg Fe per kg body weight) at appropriate time points. T_2 and T_2*-weighted MR images of mice tumor were acquired. The scan parameters were as follows: TR/TE = 400 ms/8.0 ms for T_2*-weighted flash sequence, TR/TE = 1386.5 ms/27 ms for T_2-weighted flash sequence, field of view = 6 cm, flip angle = 30°, FOV = 3.5 cm × 3.5 cm, slice thickness = 1 mm, matrix size = 256 × 256.

2.6. Histological examination

Tumor tissues and other organs were harvested 24 h after injection of normal saline, Fe_3O_4@PEG and Fe_3O_4@RGD-TRAIL. After being fixed in 10% formalin, embedded with paraffin, and sliced into 5 μm thickness, the tissue slices were stained by Prussian blue and nuclear fast red and stained with Hematoxylin and Eosin (H&E) as well.

2.7. Statistical analysis

All data were reported as mean ± SE. Significant differences were determined using Student's *t*-test where differences were considered significant when $P < 0.05$.

3. Results

3.1. Construction and characterization of Fe_3O_4@PEG and Fe_3O_4@RGD-TRAIL

The construction of Fe_3O_4@RGD-TRAIL was according to the schematic illustration in Fig. 1(A). We first synthesized the oleic acid (OA) coated iron oxide nanoparticles (Fe_3O_4@OA), the morphology, size and crystal structure of Fe_3O_4@OA were characterized by TEM. Fig. 1(B1, B2) show the as-prepared Fe_3O_4@OA are uniform and hexagonal. In addition, the high-quality crystalline nature of Fe_3O_4@OA was confirmed by XRD and SAED (Fig. S1). In order to increase biocompatibility, water-solubility and blood circulation time, the hydrophobic Fe_3O_4@OA was further coated with DSPE-PEG2000-COOH molecules [26]. Both of the Fe_3O_4@PEG and Fe_3O_4@RGD-TRAIL had a magnetic core (22 nm) −organic shell (3 nm) structure (Fig. 1(B3, B4)). The thin and uniform layer of DSPE-PEG2000-COOH was visible in TEM image after negative staining with 2% phosphotungstic acid.

RGD-TRAIL could be covalently conjugated on Fe_3O_4@PEG using the carbodiimide reaction between carboxyl groups of Fe_3O_4@PEG and amino groups of RGD-TRAIL. BCA kit test showed that approximately 39 μg RGD-TRAIL protein was coupled to per mg nanoparticles (in terms of Fe content). Fig. 2(A) shows both Fe_3O_4@PEG and Fe_3O_4@RGD-TRAIL have similar size distribution (average size of about 45 nm). The zeta potentials of Fe_3O_4@PEG and Fe_3O_4@RGD-TRAIL were −45.9 and −56.9 mV respectively, revealing Fe_3O_4@RGD-TRAIL having a higher colloidal stability.

The magnetic characteristic of the nanoprobes is significant for in vivo applications. As is shown in Fig. 2(B), the hysteresis loop at room-temperature displayed particularly high saturation magnetization of 93 and 92 emu/g Fe for Fe_3O_4@PEG and Fe_3O_4@RGD-TRAIL. In addition, the hysteresis loop of the two nanoprobes featured superparamagnetic behavior. Fig. 2(C, D) showed that the MR signal intensities were declined as the concentration of the samples increased. The corresponding relaxivity coefficient (r_2) values of Fe_3O_4@PEG and Fe_3O_4@RGD-TRAIL were 524 and 534 $mM^{-1}s^{-1}$, respectively. It was obvious that high saturation magnetization and relaxivity coefficient (r_2) tended to achieve more sensitive MRI contrast effect, while less dosage of contrast agent should be used.

3.2. Cellular targeting, cytotoxicity and uptake of Fe_3O_4@PEG and Fe_3O_4@RGD-TRAIL in vitro

It is well known that $\alpha_v\beta_3$ integrin, overexpressed in activated and proliferating endothelial cells, is a specific marker of angiogenesis in tumor progression [27]. HUVECs are generally used to check the binding of RGD peptide to $\alpha_v\beta_3$ integrin which is specially expressed on the cytomembrane of HUVECs [28,29]. Death receptors (DR) were highly expressed by various tumor cells and COLO-205 colon cancer cells were reported to overexpress DR4/DR5 [22]. The in vitro cell targeting capabilities of Fe_3O_4@RGD-TRAIL were confirmed using COLO-205 cells [30] and HUVECs treated with PBS, Fe_3O_4@PEG and Fe_3O_4@RGD-TRAIL, respectively. The cellular targeting and uptake of the nanoprobes was assessed by Prussian blue staining. Here, our results showed that Fe_3O_4@RGD-TRAIL could specifically bond with DR4/DR5 of COLO-205 cells and $\alpha_v\beta_3$ integrin of HUVECs after a certain time of

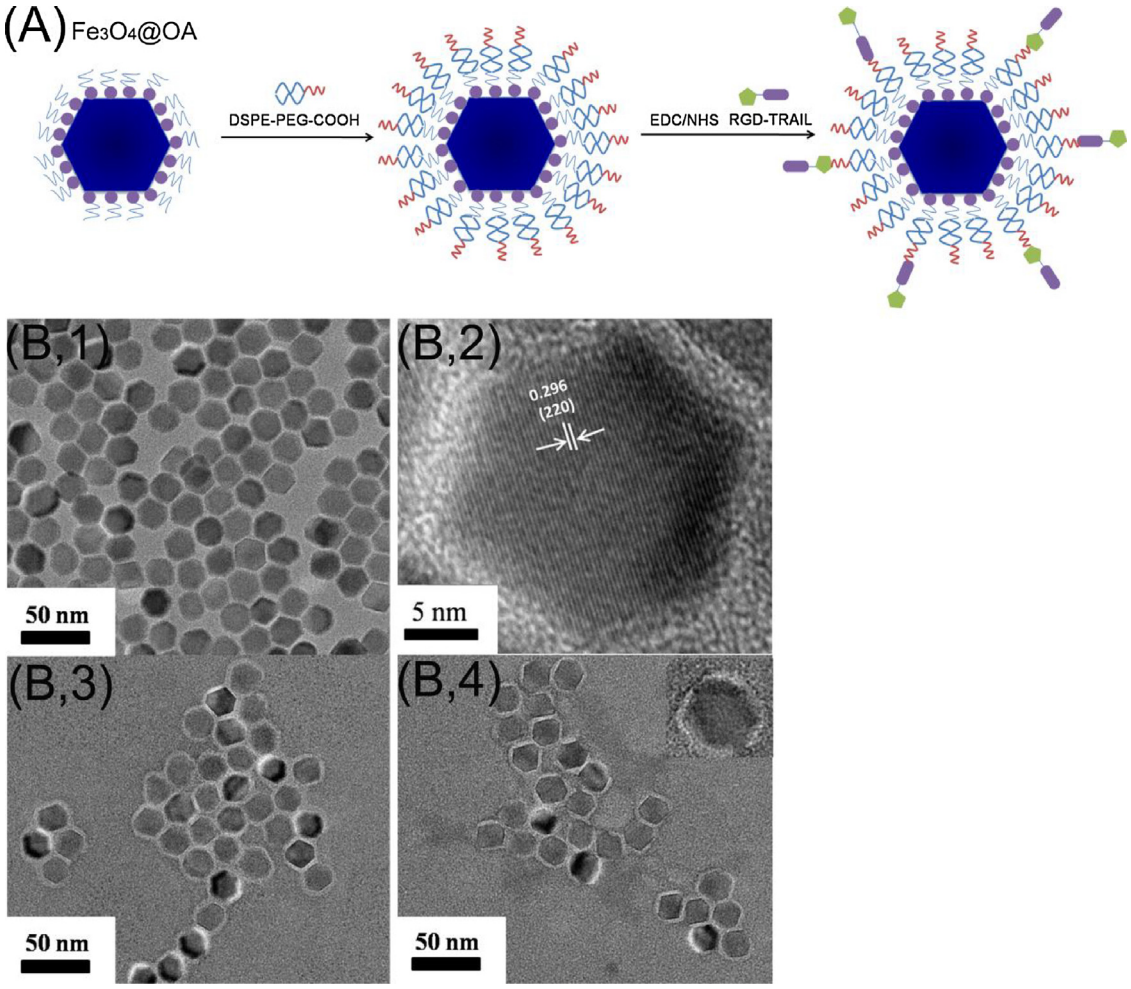

Fig. 1. (A) A schematic diagram of iron oxide nanoparticle Fe_3O_4@PEG and Fe_3O_4@RGD-TRAIL synthesis. (B,1) TEM image and (B,2) high-resolution TEM image of oleic acid modified iron oxide nanoparticles Fe3O_4@OA, TEM images of (B,3) Fe_3O_4@PEG and (B,4) Fe_3O_4@RGD-TRAIL negatively stained with 2% phosphotungstic acid to indicate the coating lipid and protein layer.

incubation (blue color marking) [Fig. 3(A, B)], while there was no distinct cellular binding for Fe_3O_4@PEG.

In addition, CCK8 assays were carried out to evaluate the cytotoxicity of Fe_3O_4@PEG and Fe_3O_4@RGD-TRAIL in vitro. Fig. 3(C, D) presented that cell viability of COLO-205 cells and HUVECs both exceeded 90% even at a relatively high incubating concentration of 60 μg Fe/ml for Fe_3O_4@PEG. Nevertheless, an appreciable toxicity was observed in COLO-205 cells at 20–60 μg Fe/ml for Fe_3O_4@RGD-TRAIL, while cell viability of HUVECs exceeded 80% even at 60 μg Fe/ml for Fe_3O_4@RGD-TRAIL. This result exhibited that after conjugation of RGD-TRAIL on the nanoprobe, the biological activity of RGD-TRAIL has been maintained. Further, Fe_3O_4@RGD-TRAIL was just cytotoxic to cancer cells as COLO-205 cells overexpressing DR4/DR5 but not to normal cells of HUVECs.

Another key consideration for in vivo application of nanoprobes is to assess the ability of escaping RES. Herein, we conducted in vitro cellular phagocytosis experiments of Fe_3O_4@PEG and Fe_3O_4@RGD-TRAIL by using RAW264.7 macrophages. Meanwhile, dimercaptosuccinic acid (DMSA)-modified nanoparticles (Fe_3O_4@DMSA) were used for comparision [18]. The cellular uptake of the nanoprobes was detected using Prussion blue staining. Representative images of macrophages after incubation 4 h with different concentration of 50 and 100 μg Fe/ml of Fe_3O_4@PEG, Fe_3O_4@RGD-TRAIL and Fe_3O_4@DMSA were shown in Fig. 4 (A, B). It could be observed that macrophages incubated with Fe_3O_4@DMSA were stained blue obviously. Whereas Fe_3O_4@PEG, Fe_3O_4@RGD-TRAIL induced non-detectable cellular uptake at 50 μg Fe/ml and significantly lower cell uptake at 100 μg Fe/ml. These results demonstrated that both the PEGylated nanoprobes drastically minimized the non-specific phagocytosis of macrophages, which would endow Fe_3O_4@RGD-TRAIL the ability to escape RES uptake to reach tumors in vivo.

3.3. *in vivo T_2-weighted MR imaging of COLO-205 tumor model*

Because of the low non-specific phagocytosis of macrophages and high targeting capacity both to DR4/DR5 of COLO-205 cells and $\alpha_v\beta_3$ integrin, the further in vivo active-target T_2 MR imaging enhancement of Fe_3O_4@RGD-TRAIL was verified. Nude mice were injected via tail vein with Fe_3O_4@PEG and Fe_3O_4@RGD-TRAIL at a dose of 17.5 mg Fe/kg and imaged by a 7.0 T micro-MRI. Clearly, Fe_3O_4@PEG and Fe_3O_4@RGD-TRAIL both induced MR contrast enhancement of the COLO-205 tumors (Fig. 5A). A fraction of the tumor turned dark 3 h post-injection of both nanoprobes. In the course of time, the passively-targeted Fe_3O_4@PEG-induced MR signal in the tumor region was partly darken and gradually weakened 24 h post-injection and mainly disappeared 48 h later, meaning the inhomogeneous distribution, fast EPR effect and clearance of Fe_3O_4@PEG in vivo. In comparison, after injection of the actively-targeted Fe_3O_4@RGD-TRAIL, the MR signal reached strongest 24 h later and was relatively uniform in tumor site as well as the signal still existed as long as 48 h. The enhancement intensity of tumor

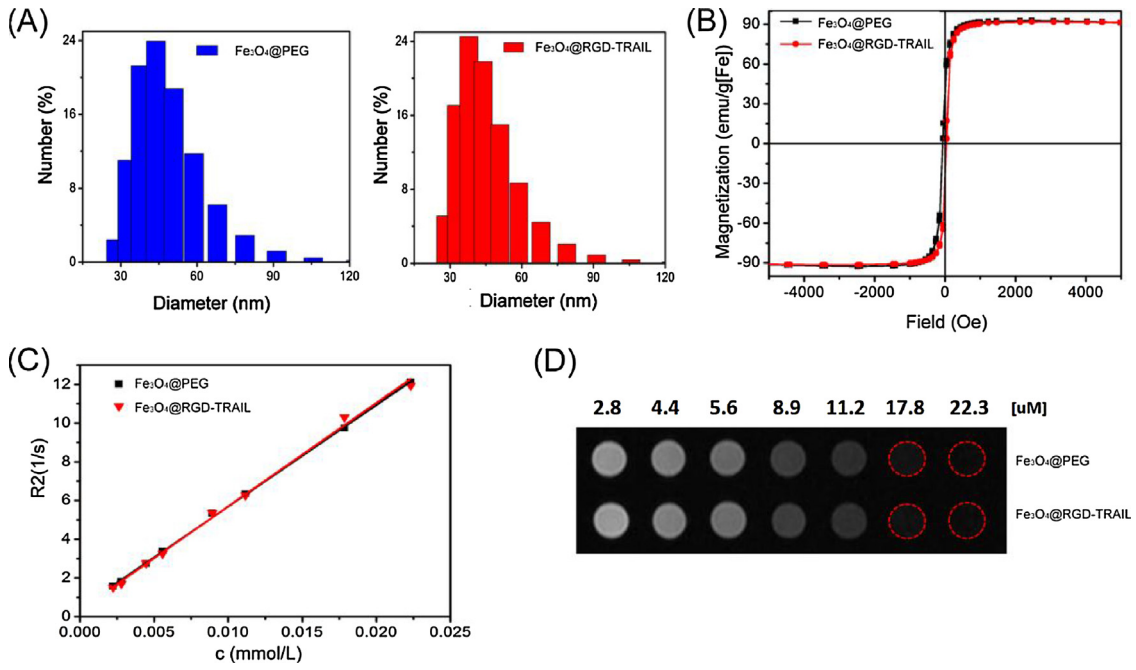

Fig. 2. (A) DLS data of Fe_3O_4@PEG and Fe_3O_4@RGD-TRAIL in water. (B) M-H curves of Fe_3O_4@PEG and Fe_3O_4@RGD-TRAIL. (C) Relaxation rate and (D) T2-weighted MR image of Fe_3O_4@PEG and Fe_3O_4@RGD-TRAIL upon iron concentration measured by a 1.5T MR scanner. The red dotted circles displayed the black MR images as the iron concentration increased. (For interpretation of the references to colour in this figure legend, the reader is referred to the web version of this article.)

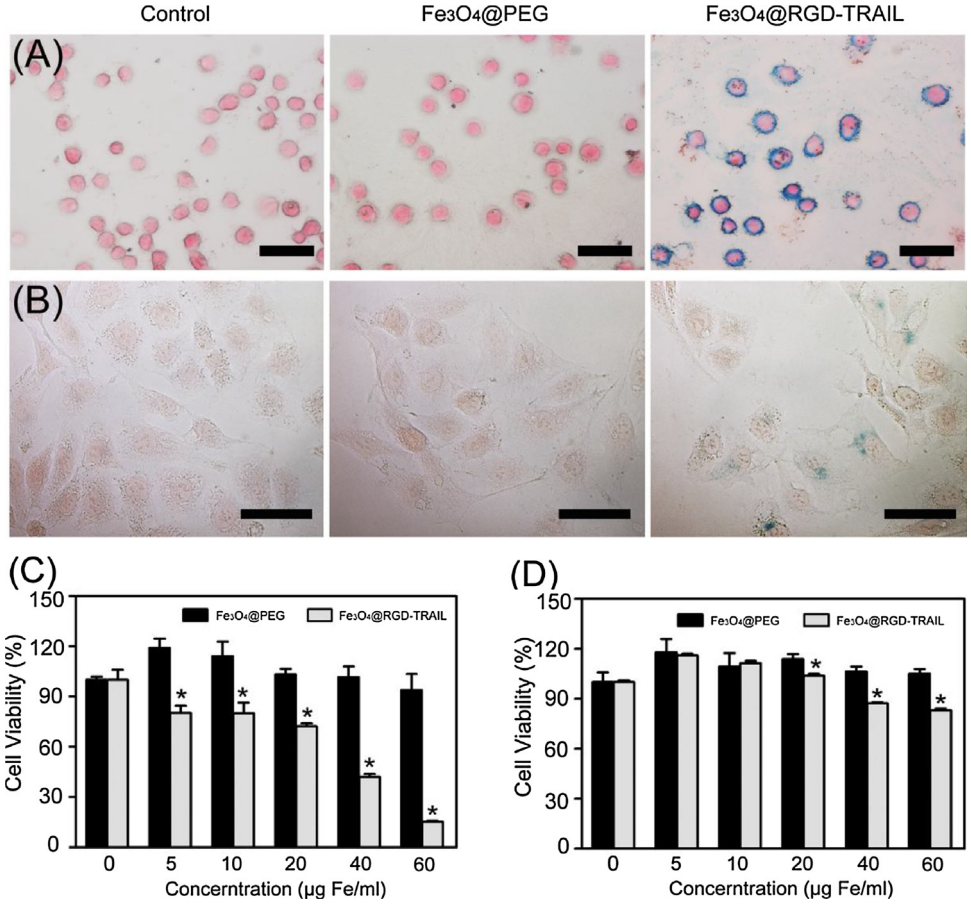

Fig. 3. Cellular targeting testing with Nuclear fast red and Prussian blue double staining for (A) COLO-205 cells and (B) HUVECs after treatment with PBS, Fe_3O_4@PEG and Fe_3O_4@RGD-TRAIL at the concentration of 100 μg Fe/ml. The black bar represented 50 μm. In vitro cytotoxicity test of Fe_3O_4@PEG and Fe_3O_4@RGD-TRAIL for (C) COLO-205 cells and (D) HUVECs. The viability of the cells was determined by cck8 assay after incubation with various concentrations of Fe for 24 h (n = 5). For (C) COLO-205 cells, after incubation with the two nanoprobes, cell viability showed significant difference (P values were 0.0049, 0.0334, 0.0013, 0.0008 and 0.0012 for 5–60 μg Fe/ml, respectively). For (D) HUVECs, cell viability showed significant difference at 20–40 μg Fe/ml (P values were 0.0349, 0.004 and 0.002, respectively). (For interpretation of the references to colour in this figure legend, the reader is referred to the web version of this article.)

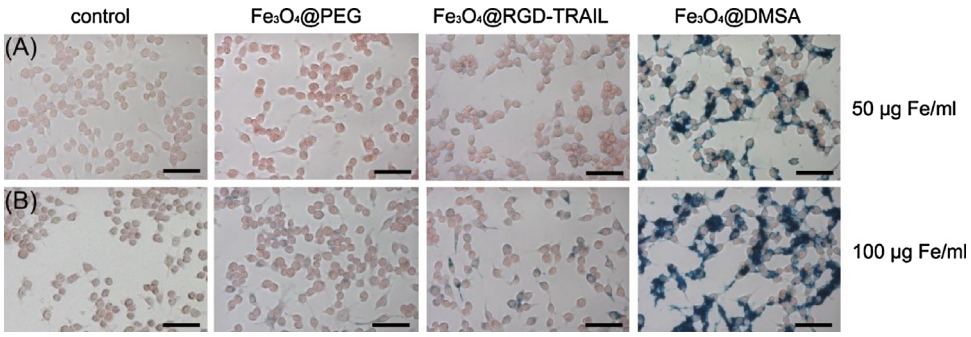

Fig. 4. Cellular uptake testing with Nuclear fast red and Prussian blue double staining for macrophages of RAW264.7 after 4 h treatment with Fe_3O_4@PEG, Fe_3O_4@RGD-TRAIL and Fe_3O_4@DMSA at the concentrations of (A) 50 μg Fe/ml and (B) 100 μg Fe/ml. The black bar represented 50 μm. (For interpretation of the references to colour in this figure legend, the reader is referred to the web version of this article.)

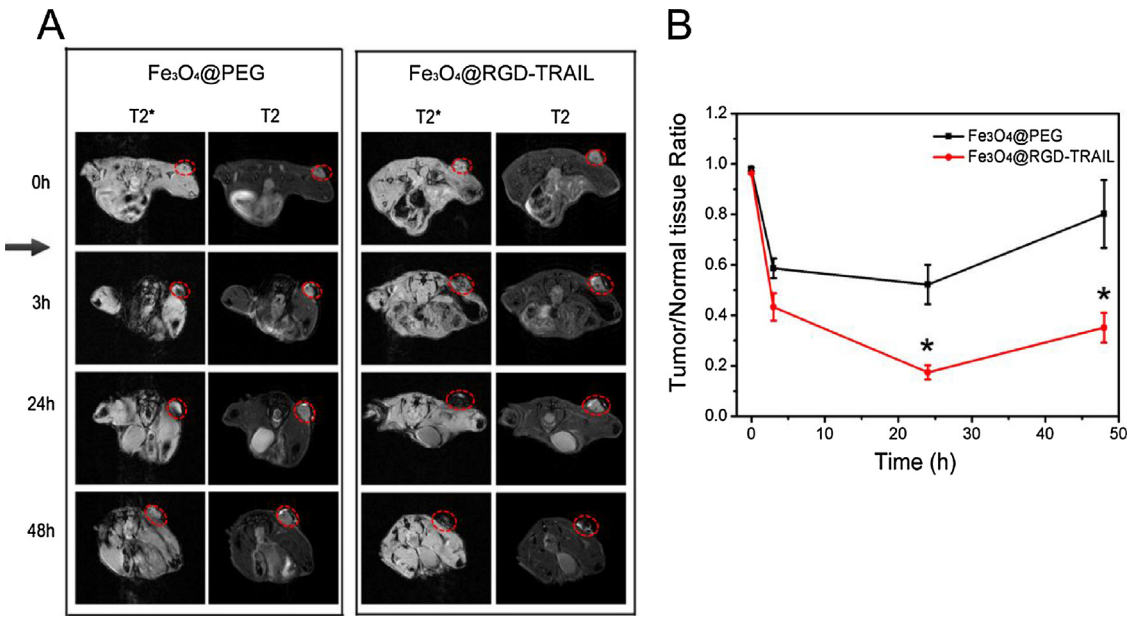

Fig. 5. (A) T2 and T2*-weighted MR images of mice tumor acquired before and after single tail vein injection of Fe_3O_4@PEG and Fe_3O_4@RGD-TRAIL (17.5 mg Fe/kg body weight) at different time points using a 7 T MR scanner. The red dotted line displayed the tumor site. (B) TNR of MRI-based average signal in Fe_3O_4@PEG and Fe_3O_4@RGD-TRAIL groups at corresponding time points to Figure (A). The data of (B) is shown as mean ± SE (n = 3). TNR values showed notable difference at 24 h and 48 h after injection of two nanoprobes (P = 0.0138 and P = 0.0369, respectively). (For interpretation of the references to colour in this figure legend, the reader is referred to the web version of this article.)

tissue was also analyzed quantitatively based on Tumor/Normal tissue Ratio (TNR) values between the tumor and the adjacent normal muscles (Fig. 5B). These results proved that the Fe_3O_4@RGD-TRAIL owned the MR imaging ability of improved and prolonged tumor targeting.

3.4. Distribution of Fe_3O_4@PEG and Fe_3O_4@RGD-TRAIL in vivo and histological analysis

To further confirm the distribution of the two nanoprobes in vivo, the main organs and tumor tissues from the experimental mice were harvest 24 h post-injection (Fe_3O_4@PEG or Fe_3O_4@RGD-TRAIL). Prussian blue staining was used to verify the existence of Fe in tissues. Fig. 6 showed that obvious blue spots appeared in tumor as well as in liver and spleen both of the passively- and actively-targeted groups, suggesting that the two nanoprobes can target to COLO-205 tumor with little undesired phagocytosis by RES. No significant accumulation of nanprobe was detected in other major organs (Fig. S2). In addition, hematoxylin and eosin (H&E) stains of major organs and tumor tissues showed no evidence of any adverse effect due to the nanoprobes (Fig. S3).

4. Discussion

Construction of an ultrasensitive and highly precise probe for tumor imaging is the first step in tumor theranostics. In order to maximize the diagnostic sensitivity and minimize the influence induced by heterogeneity of tumor microenvironment, the probe should be designed with high performance and multi-targeted ability that can simultaneously target multiple tumor-associated receptors. In this work, we demonstrate a RGD-TRAIL conjugated iron oxide nanoprobe for T2-weighted magnetic resonance molecular imaging of COLO-205 colorectal cancer. To greatly improve the cancer detection efficacy, several key factors for the nanoprobe are established as follows.

The magnetic property of the nanoprobe is the most important for successful diagnosis of tumor. Although the doping of metal ion such as Mn, Ni, Zn and Co can improve the magnetic susceptibility of conventional $Fe_3O_4$and γ-Fe_2O_3 [31,32], it is still controversial to use them in clinical due to potential toxicity for these elements [33]. Up to now, magnetic iron oxide nanoparticle is unique as nanomaterial approved by FDA for use as MRI contrast agent. In this regard, the nanoprobe was made of iron oxide and free from

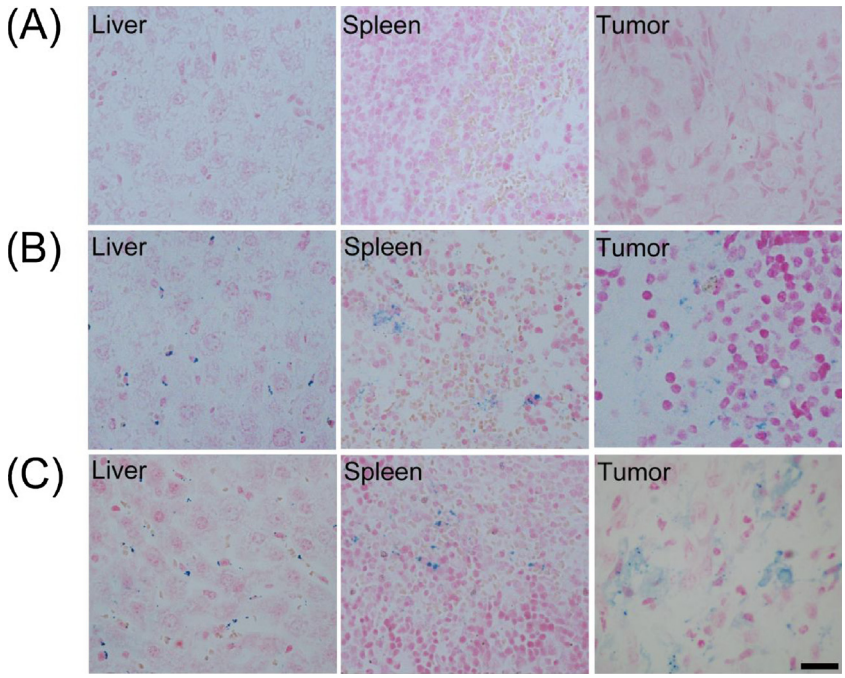

Fig. 6. Nuclear fast red and Prussian blue double staining images (400×) of phagocytosis organs and tumor after intravenous administration of (A) normal saline, (B) Fe_3O_4@PEG, (C) Fe_3O_4@RGD-TRAIL for 24 h. The black bar represented 50 μm. (For interpretation of the references to colour in this figure legend, the reader is referred to the web version of this article.)

toxic elements. The nanoprobe of Fe_3O_4@RGD-TRAIL was proven to exhibit extremely high relaxation property (r_2 = 534 $mM^{-1}s^{-1}$) and saturation magnetization value (M_s = 92 emu/g Fe) which is much higher than that of Feridex (r_2 = 133 $mM^{-1}s^{-1}$, Ms = 64.4 emu/g Fe) in previous report [15]. It is also noteworthy that the r_2 of Fe_3O_4@RGD-TRAIL is higher than that of previously reported superparamagnetic nanoparticles [15,23]. The outstanding magnetism ensures the possibility of the nanoprobe as MRI contrast agent for tumor diagnosis in vivo.

The surface modification of the nanoprobe is also vitally important for efficient in vivo circulation. As a common method for reducing uptake by RES and prolonging blood circulation, PEGylation of the hydrophobic iron oxide nanoparticle was realized by an amphiphilic DSPE-PEG-COOH through hydrophobic interaction. The obtained water-soluble nanoprobe was monodispersed with an obvious core-shell structure (Fig. 1(B3, B4)), narrow size distribution and good colloidal stability (Fig. 2A). On account of the lipid-PEG layer with excellent biocompatibility, the nanoprobe exhibited no obvious cytotoxicity to normal cells (Fig. 3D), and was observed to have a slight phagocytosis by macrophage both in vitro and in vivo (Fig. 4, 6). These advantages of the nanoprobe endow them high effectiveness as contrast agent for in vivo MR imaging at a relatively low dose.

Since EPR effect is the basis of passive targeting for nanoparticles, it should be taken into account that permeability of tumor vessels is heterogeneous causing inhomogenous extravasation and distribution of nanomaterials. The T2-weighted MR imaging using Fe_3O_4@PEG in our study also exhibited inhomogenous signal enhancement in COLO-205 tumor (Fig. 5A). To further improve the sensitivity and specificity of tumor imaging, a bispecific protein RGD-TRAIL was selected to decorate the nanoprobe, realizing ultrasensitive MR molecular imaging. "RGD-TRAIL" enables the nanoprobe to simultaneously target tumor neovascular endothelium and tumor cells. Thus, this nanoprobe might be useful in detection of $\alpha_v\beta_3$ and $\alpha_v\beta_5$ intergrins in tumor neovascular and DR4/DR5 positive tumor (Fig. 3 (A, B)). The results of MR imaging after injection of the dual-targeted Fe_3O_4@RGD-TRAIL showed a relatively uniform distribution, stronger signal and longer existence in tumor region compared with the passive targeted Fe_3O_4@PEG (Fig. 5A). In addition, the enhanced signal quantitatively measured as TNR values showed notable difference at 24 h and 48 h after injection of two nanoprobes ($P < 0.05$, Fig. 5B), which implied the greatly improved sensitivity and efficiency of tumor imaging by dual-targeted nanoprobe.

As RGD-TRAIL has been proved to be a promising candidate for cancer treatment by inducing tumor selective apoptosis [22,30], and in vitro toxicity experiment results in this study also showed Fe_3O_4@RGD-TRAIL resulted in COLO-205 tumor cells death and negligible toxicity to normal cells (Fig. 3 (C, D)), the RGD-TRAIL conjugated nanoprobe could further provide opportunities both in monitoring and evaluation of the tumor treatment by RGD-TRAIL.

Nowdays, an evolutionary technique such as phage display has been employed to identify cell- or tissue – homing peptides [34,35]. As phage libraries provide an inexhaustible reservoir of new ligands against tumor cells and tissues, these homing peptides can replace RGD-TRAIL to allow the nanoprobe to realize targeting imaging of other cells and tissues, such as rat mesenchymal stem cells [34] and SKBR-3 breast cancer cells [35].

5. Conclusion

In summary, we have successfully developed a novel molecular imaging technique for dual-targeted magnetic resonance imaging of COLO-205 colorectal cancer by using a monodispersed nanoprobe with high performance. We demonstrated that this nanoprobe showed outstanding magnetism, excellent biocompatibility, dual-targeting capacity, strong ability to resist against the non-specific phagocytosis and high sensitivity/efficiency of tumor imaging in vivo. Therefore, we believe that this RGD-TRAIL conjugated nanoprobe is suitable as a multi-targeted contrast agent for magnetic resonance molecular imaging of cancer, and since RGD-TRAIL can selectively induce tumor apoptosis, it could further provide opportunities both in cancer diagnosis and medication guidance.

Conflict of interest

The authors declare no competing financial interest.

Acknowledgements

This research was supported by the National Key Research and Development Program of China (No. 2017YFA0205502), the National Basic Research Program of China (973 program No. 2013CB733800), National Natural Science Foundation of China (No. 81571806, 81671820, 81301870), the Jiangsu Provincial Special Program of Medical Science (BL2013029), and the Fundamental Research Funds for the Central Universities.

Appendix A. Supplementary data

Supplementary data associated with this article can be found, in the online version, at https://doi.org/10.1016/j.colsurfb.2017.10.059.

References

[1] V. Wagner, A. Dullaart, A.K. Bock, A. Zweck, The emerging nanomedicine landscape, Nat. Biotechnol. 24 (10) (2006) 1211–1217.
[2] R.R. Qiao, C.H. Yang, M.Y. Gao, Superparamagnetic iron oxide nanoparticles: from preparations to in vivo MRI applications, J. Mater. Chem. 19 (35) (2009) 6274–6293.
[3] H.B. Na, I.C. Song, T. Hyeon, Inorganic nanoparticles for MRI contrast agents, Adv. Mater. 21 (21) (2009) 2133–2148.
[4] L. Song, F. Zang, M. Song, et al., Effective PEGylation of Fe3O4 nanomicelles for in vivo MR imaging, J. Nanosci. Nanotechnol. 15 (6) (2015) 4111–4118.
[5] D. Kokuryo, Y. Anraku, A. Kishimura, et al., SPIO-PICsome: development of a highly sensitive and stealth-capable MRI nano-agent for tumor detection using SPIO-loaded unilamellar polyion complex vesicles (PICsomes), J. Control. Release 169 (3) (2013) 220–227.
[6] N. Lee, Y. Choi, Y. Lee, et al., Water-dispersible ferromagnetic iron oxide nanocubes with extremely high r2 relaxivity for highly sensitive in vivo MRI of tumors, Nano Lett. 12 (6) (2012) 3127–3131.
[7] B.H. Kim, N. Lee, H. Kim, et al., Large-scale synthesis of uniform and extremely small-sized iron oxide nanoparticles for high-resolution T1 magnetic resonance imaging contrast agents, J. Am. Chem. Soc. 133 (32) (2011) 12624–12631.
[8] Z. Wang, R. Qiao, N. Tang, et al., Active targeting theranostic iron oxide nanoparticles for MRI and magnetic resonance-guide focused ultrasound ablation of lung cancer, Biomaterials 127 (2017) 25–35.
[9] Q. Mu, F.M. Kievit, R.J. Kant, et al., Anti-HER2/neu peptide-conjugated iron oxide nanoparticles for targeted delivery of paclitaxel to breast cancer cells, Nanoscale 7 (43) (2015) 18010–18024.
[10] K. Hayashi, M. Nakamura, W. Sakamoto, et al., Superparamagnetic nanoparticle clusters for cancer theranostics combining magnetic resonance imaging and hyperthermia treatment, Theranostics 3 (6) (2013) 366–376.
[11] M. Boucher, F. Geffroy, S. Preveral, et al., Genetically tailored magnetosomes used as MRI probe for molecular imaging of brain tumor, Biomaterials 121 (2017) 167–178.
[12] S.C. Wu, Y.J. Chen, H.C. Wang, et al., Bispecific antibody conjugated manganese-based magnetic engineered iron oxide for imaging of HER2/neu- and EGFR- expressing tumors, Theranostics 6 (1) (2016) 118–130.
[13] J. Xie, C.Z. Yan, Y. Zhang, N. Gu, Shape evolution of multibranched Mn-Zn ferrite nanostructures with high performance: a transformation of nanocrystals into nanoclusters, Chem. Mater. 25 (18) (2013) 3702–3709.
[14] J. Park, E. Lee, N.M. Hwang, et al., One-nanometer-scale size-controlled synthesis of monodisperse magnetic iron oxide nanoparticles, Angew. Chem. Int. Ed. Engl. 44 (19) (2005) 2873–2877.
[15] N. Lee, H. Kim, S.H. Choi, et al., Magnetosome-like ferromagnetic iron oxide nanocubes for highly sensitive MRI of single cells and transplanted pancreatic islets, Proc. Natl. Acad. Sci. U. S. A. 108 (7) (2011) 2662–2667.
[16] H. Yang, T. Ogawa, D. Hasegawa, et al., Synthesis and magnetic properties of monodisperse magnetite nanocubes, J. Appl. Phys. 103 (7) (2008) (07D526).
[17] V.P. Torchilin, Structure and design of polymeric surfactant-based drug delivery systems, J. Control. Release 73 (2-3) (2001) 137–172.
[18] J. Xie, Y. Zhang, C.Y. Yan, et al., High-performance PEGylated Mn-Zn ferrite nanocrystals as a passive-targeted agent for magnetically induced cancer theranostics, Biomaterials 35 (2014) 9126–9136.
[19] S. Rampersaud, J. Fang, Z. Wei, et al., The effect of cage shape on nanoparticle-based drug carriers: anticancer drug release and efficacy via receptor blockade using dextran-coated iron oxide nanocages, Nano Lett. 16 (12) (2016) 7357–7363.
[20] X. Sun, B. Dong, H. Xu, et al., Amphiphilic silane modified multifunctional nanoparticles for magnetically targeted photodynamic therapy, ACS Appl. Mater. Interfaces 9 (13) (2017) 11451–11460.
[21] R.K. Jain, T. Stylianopoulos, Delivering nanomedicine to solid tumors, Nat. Rev. Clin. Oncol. 7 (11) (2010) 653–664.
[22] L. Cao, P. Du, S.H. Jiang, G.H. Jin, Q.L. Huang, Z.C. Hua, Enhancement of antitumor properties of TRAIL by targeted delivery to the tumor neovasculature, Mol. Cancer Ther. 7 (4) (2008) 851–861.
[23] J. Xie, C.Y. Yan, Y. Yan, L. Chen, L.N. Song, F.C. Zang, Y.L. An, G.J. Teng, N. Gu, Y. Zhang, Multi-modal Mn-Zn ferrite nanocrystals for magnetically-induced cancer targeted hyperthermia: a comparison of passive and active targeting effects, Nanoscale 8 (38) (2016) 16902–16915.
[24] M.J. Song, Y. Zhang, S.L. Hu, L.N. Song, J.L. Dong, Z.P. Chen, Influence of morphology and surface exchange reaction on magnetic properties of monodisperse magnetite nanoparticles, Coll. Surf. A Physicochem. Eng. Asp. 408 (2012) 114–121.
[25] A.E. Harvey, J.A. Smart, E.S. Amis, Simultaneous spectrophotometric determination of iron(II) and total iron with 1, 10-phenanthroline, Anal. Chem. 27 (1955) 26–29.
[26] S. Tong, S.J. Hou, Z.L. Zheng, et al., Coating optimization of superparamagnetic iron oxide nanoparticles for high T2 relaxivity, Nano Lett. 10 (2010) 4607–4613.
[27] M. Friedlander, C.L. Theesfeld, M. Sugita, et al., Involvement of integrins $\alpha_v\beta_3$ and $\alpha_v\beta_5$ in ocular neovascular diseases, Proc. Natl. Acad. Sci. U. S. A. 93 (18) (1996) 9764–9769.
[28] C.F. Zhang, M. Jugold, E.C. Woenne, et al., Specific targeting of tumor angiogenesis by RGD-conjugated ultrasmall superparamagnetic iron oxide particles using a clinical 1. 5-T magnetic resonance scanner, Cancer Res. 67 (4) (2007) 1555–1562.
[29] Z.Y. Jia, L.N. Song, F.C. Zang, et al., Active-targeted T1-weighted MR imaging of tiny hepatic tumor via RGD modified ultra-small Fe3O4 nanoprobes, Theranostics 6 (11) (2016) 1780–1791.
[30] L. Duan, F. Yang, W. He, et al., A multi-gradient targeting drug delivery system based on RGD-L-TRAIL-labled magnetic microbubbles for cancer theranostics, Adv. Funct. Mater. 26 (45) (2016) 8313–8324.
[31] Y.W. Jun, J.H. Lee, J. Cheon, Chemical design of nanoparticle probes for high performance magnetic resonance imging, Angew. Chem. Int. Ed. 47 (2008) 5122–5135.
[32] J.T. Jang, H. Nah, J.H. Lee, et al., Critical enhancements of MRI contrast and hyperthermia effects by dopant-controlled magnetic nanoparticles, Angew. Chem. Int. Ed. 48 (2009) 1234–1238.
[33] C. Wang, K. Cheng, L. Zhou, et al., Evaluation of long-term toxicity of oral zinc oxide nanoparticles and zinc sulfate in Mice, Biol. Trace Elem. Res. (2017) 1–7.
[34] K. Ma, D.D. Wang, Y.Y. Lin, et al., Synergetic targeted delivery of sleeping-beauty transposon system to mesenchymal stem cells using LPD nanoparticles modified with a phage-displayed targeting peptide, Adv. Funct. Mater. 23 (2013) 1172–1181.
[35] G. Abbineni, S. Modali, B. Safiejko-Mroczka, et al., Evolutionary selection of new breast cancer cell-targeting peptides fully displayed on the major coat and their effects on actin dynamics during cell internalization, Mol. Pharm. 7 (5) (2010) 1629–1642.